A mixed finite element discretization scheme for a concrete carbonation model with concentration-dependent porosity

EINDHOVEN UNIVERSITY OF TECHNOLOGY
Department of Mathematics and Computer Science

CASA-Report 11-49
September 2011

A mixed finite element discretization scheme for a concrete carbonation model with concentration-dependent porosity

by

F.A. Radu, A. Muntean, I.S. Pop, N. Suciu, O. Kolditz

Centre for Analysis, Scientific computing and Applications
Department of Mathematics and Computer Science
Eindhoven University of Technology
P.O. Box 513
5600 MB Eindhoven, The Netherlands
ISSN: 0926-4507

A mixed finite element discretization scheme for a concrete carbonation model with concentration-dependent porosity

Florin A. Radu[1,2*], Adrian Muntean[3,4], Iuliu S. Pop[4], Nicolae Suciu[2,5], Olaf Kolditz[1,6]

[1] Division of Computational Environmental Systems, UFZ-Helmholtz Center for Environmental Research
Permoserstr. 15, D-04318 Leipzig, Germany

[3] Institute for Complex Molecular Systems (ICMS), Eindhoven University of Technology,
P. O. Box 513, 5600 MB Eindhoven, The Netherlands

[4] Department of Mathematics and Computer Science, Eindhoven University of Technology,
P. O. Box 513, 5600 MB Eindhoven, The Netherlands

[2] Mathematics Department, Applied Mathematics 1, Friedrich-Alexander University of Erlangen-Nuremberg
Martensstrasse 3, D-91058 Erlangen, Germany

[5] Tiberiu Popoviciu Institute of Numerical Analysis, Romanian Academy
Fantanele 57, 400320 Cluj-Napoca, Romania

[6] Technische Universität Dresden, Helmholtzstr. 10, D-01056 Dresden, Germany

e-mails: {*florin.radu, olaf.kolditz*}*@ufz.de,* {*a.muntean, i.pop*}*@tue.nl, suciu@am.uni-erlangen.de*

Abstract

We discuss a prototypical reaction-diffusion-flow problem in saturated/unsaturated porous media. The special features of our problem are: the reaction produces water and therefore the flow and transport are coupled in both directions and moreover, the reaction may alter the microstructure. This means we have a variable porosity in our model. For the spatial discretization we propose a mass conservative scheme based on the mixed finite element method (MFEM). The scheme is semi-implicit in time. Error estimates are obtained for some particular cases. We apply our finite element methodology for the case of concrete carbonation – one of the most important physico-chemical processes affecting the durability of concrete.

1 Introduction

We consider the following prototypical reaction–diffusion problem: A gaseous species $\tilde{\mathrm{A}}$ penetrates a non-saturated porous medium via the air phase of its pore space and quickly dissolves in the pore water where $\tilde{\mathrm{A}}$ reacts very fast with a species $\tilde{\mathrm{B}}$. The species $\tilde{\mathrm{B}}$ becomes available from the solid matrix by a dissolution mechanism. The reaction produces a species $\tilde{\mathrm{C}}$ which precipitates to the porous matrix. The process can be summarized as

$$\tilde{\mathrm{A}}(\mathrm{g} \to \mathrm{ag}) + \tilde{\mathrm{B}}(\mathrm{s} \to \mathrm{aq}) \to \tilde{\mathrm{C}}(\mathrm{aq} \to \mathrm{s}) + \mathrm{H_2O}. \tag{1}$$

If the species $\tilde{\mathrm{A}}$, $\tilde{\mathrm{B}}$, and $\tilde{\mathrm{C}}$ are $\mathrm{CO_2}$, $\mathrm{Ca(OH)_2}$, and respectively, $\mathrm{CaCO_3}$, then the reaction is called carbonation and is one of the most important processes limiting the service life of concrete structures. We refer to [18, 26] for a concise description of the details of the involved cement chemistry, of existing

*Part of the work of F. A. Radu was supported by the IWAS project, which is funded by the Federal Ministry of Education and Research Germany (BMBF). This support is gratefully acknowledged.

isoline models for concrete carbonation, and of the parametric regimes when both the reaction rate of (1) and the Henry-type transfer of species $\tilde{\mathrm{A}}$ from the gaseous phase to the liquid phase (and vice versa) can be assumed to be fast. For closely related settings arising in geochemistry, see e. g. [8, 25].

Scenarios described by reaction (1) can incorporate changes in the pore volume induced by a difference in the densities of $\tilde{\mathrm{B}}$ and $\tilde{\mathrm{C}}$. Such structural changes may locally clog the pores by a strong localized precipitation of $\tilde{\mathrm{C}}$. In this sense we refer to [16, 21, 22, 23] for the derivation, analysis and upscaling of mathematical models leading to dynamic, solution dependent change of the pore volumes due to dissolution and precipitation processes, or biofilm growth encountered at the pore scale. Note also that due to (1) some water is produced as well. Assuming (1) to be fast (in the spirit of [11] (chapter II.5), e.g.), we expect the occurrence of localized productions of water. If, on the other hand, the production is also strong, then a barrier of water might stop the penetration of the gaseous species $\tilde{\mathrm{A}}$ [18]. The challenge is to investigate under which circumstances (i.e. parameter ranges, boundary conditions, model for porosity, etc.) the clogging of the pores and the water barrier effect can take place.

The need of an adequate approximation of the fluid flow by mixed finite element method (MFEM) has been recognized in the water resources literature since several decades, see, e.g., [19]. This method offers the advantage of local mass conservation and continuous flux approximations over the element faces. However, for associated solute transport problems normally conventional methods are applied, e.g. conforming finite element method [3, 5], finite volume [15, 24], discontinuous Galerkin [30] or method of characteristics [14]. In [27, 28] a scheme based on MFEM is proposed also for multicomponent, reactive solute transport in soil. More precisely, the lowest order Raviart-Thomas elements are used. There, the coupling was only in one direction, so the flow equation could be solved separately. In this work we extend the scheme presented in [27, 28] for reactive transport in porous media with concentration-dependent porosity. Thus we introduce and analyze a novel formulation of a coupled reactive multicomponent transport model and flow with variable porosity in a MFEM setting.

The paper is structured as follows. In Section 2, we present the model equations for the reaction-diffusion-flow problem with concentration-dependent porosity indicated above. The main results of the paper are the subject of Section 3 (a numerical scheme for a reduced PDE system, including some error estimates and convergence of the method). Finally, we solve the reduced PDE system and illustrate its behavior in the fast-reaction limit in Section 4. We conclude with some discussions in Section 5.

2 Model equations

We consider a porous medium occupying a domain Y in $\mathbb{R}^d$, $d = 2$ or 3 and having the boundary ∂Y. We denote by Ω a reference elementary volume of our (homogeneous) material, and by Ω_p and Ω_s the volume occupied by the pores and the matrix volume, respectively. Denote by $|\Omega'|$ the volume of a region $\Omega' \subset \Omega$. Then $\phi := \frac{|\Omega_p|}{|\Omega|}$ is the porosity of the medium, while $\phi_s := 1 - \phi$ is the corresponding solid fraction. Furthermore, $\phi_w := \frac{|\Omega_w|}{|\Omega_p|}$ and $\phi_g := \frac{|\Omega_g|}{|\Omega_p|}$ is the water and respectively gas fraction. Clearly, $\phi_w + \phi_g = 1$. Furthermore, we denote by a, A, b, B, c, and C the (microscopic) molar concentrations of the species $\tilde{\mathrm{A}}(\mathrm{g})$, $\tilde{\mathrm{A}}(\mathrm{aq})$, $\tilde{\mathrm{B}}(\mathrm{s})$, $\tilde{\mathrm{B}}(\mathrm{ag})$, $\tilde{\mathrm{C}}(\mathrm{s})$, and $\tilde{\mathrm{C}}(\mathrm{ag})$. Further, let $J = (0, T]$ the time interval, with T denoting a finite end time.

2.1 Productions by reaction (1), precipitation, and dissolution

We refer to [11] for the mathematical modeling of reactive porous media flows. In particular, dissolution and precipitation Darcy-scale models are proposed in [12]. Such models can be derived rationally from pore scale models (as proposed e. g. in [10, 22]) by upscaling techniques [16, 21], allowing to include the variations in the porosity (including clogging) as the result of precipitation or dissolution. To maintain the discussion brief we let γ denote the reaction rate associated to (1). Here we assume

$$\gamma := r\phi\phi_w A^p B^q, \tag{2}$$

where the constant $r > 0$ has here a very large value. $p, q \in \mathbb{R}$ are partial orders of reaction that are equal or greater than unity. Throughout this work we take $p = q = 1$. The equation (2) is sometimes called *generalized mass-action law*. Large values of r indicate the fast-reaction regime. As production rates by reaction we make use of

$$\gamma_i = \sigma_i m_i \gamma, \tag{3}$$

where σ_i is the involved stoichiometric coefficient, while m_i is the molecular weight of the species i. In this paper we consider reaction (1), therefore we have $\sigma_i = 1$ for all species $\tilde{A}, \tilde{B}$ and $\tilde{C}$. The production rates by precipitation and dissolution f_{Prec} and f_{Diss} are defined by means of deviations from known equilibrium configurations. In this paper we choose $f_{\mathrm{Prec}}(E) := S_{\mathrm{Prec}}(E - E_{p,eq})$ and $f_{\mathrm{Diss}}(E) := S_{\mathrm{Diss}}(E_{d,eq} - E)$, where E is the molecular concentration of a given species. Here S_{Prec} and S_{Diss} are given constants, while $E_{d,eq}$ and $E_{p,eq}$ are known equilibrium profiles. By the choice above, a species $\tilde{E}$ is dissolved as long as the concentration E is smaller than $E_{d,eq}$, and precipitates when the concentration E exceeds $E_{p,eq}$ (see also [10, 12, 22]).

2.2 The water flux

For the mathematical modeling of the flow in porous media we follow [6]. Assuming that the gas pressure is constant inside the pores, the flux of water $\mathbf{q}$ takes the form

$$\mathbf{q} = -K(\phi\phi_w)\nabla(p + z), \tag{4}$$

where $K(\phi\phi_w) = K_S \phi k(\phi_w)$, whereas K_S stands for the permeability of the saturated porous material and $k(\phi_w)$ is the hydraulic conductivity, which is a function of ϕ_w. z denotes the height against the gravitational direction. In this paper we assume the air pressure to be constant, and hence, $p = -p_c$, with p_c denoting the capillary pressure. At equilibrium conditions (and *fixed* porosity), the water fraction ϕ_w is a function of the capillary pressure:

$$\phi_w = \phi_w(p_c). \tag{5}$$

Typical curves are provided in the literature, such as the van Genuchten-Mualem class, or Brooks and Corey. In this paper we use the van Genuchten-Mualem parameterization [13, 20] in the form

$$\phi_w(p) = \phi_{w,\max}(1 + (-\alpha p)^n)^{-m}, \tag{6}$$

$$k(\phi_w) = \sqrt{\phi_w}(1 - (1 - \phi_w^{\frac{1}{m}})^m)^2, \qquad m = 1 - \frac{1}{n}. \tag{7}$$

2.3 Henry-type transfer at air/liquid interfaces

The species $\tilde{\mathrm{A}}$ enters the porous media via the air-filled parts of the pores and dissolves in water passing through microscopic air/liquid interfaces. The easiest way to model this transfer from the air phase to the water phase and vice versa is to rely on Raoult's law or on Henry's law. For modeling arguments, see [17] or any textbook on physical chemistry. The use of Henry's law implies that terms like

$$\pm P(H\phi\phi_w A - \phi\phi_g a) \tag{8}$$

will enter the right-hand side of the mass-balance equations for the concentrations a and A. In (8), P is a mass-transfer coefficient, which is in most cases unknown and needs to be identified for instance via a homogenization approach, and H is the Henry constant, whose value can be read off from existing databases. Nevertheless, in this work we focus only on situations where the mass transfer across liquid-air interfaces is very fast, i.e. $P \to \infty$ enforcing that

$$H\phi_w A \approx \phi_g a. \tag{9}$$

2.4 Macroscopic balance laws

The set of mass-balance equations describing the situation depicted previously reads:

$$
\begin{aligned}
(\phi\phi_w)_t + \nabla\cdot\mathbf{q} &= \frac{\phi\phi_w}{\rho} rAB, && (10)\\
\mathbf{q} &= -K_S\phi k(\phi_w)\nabla(p+z), && (11)\\
(\phi\phi_w A)_t + \nabla\cdot(-D_A\phi\phi_w\nabla A + \mathbf{q}A) &= -P(H\phi\phi_w A - \phi\phi_g a) - r\phi\phi_w m_A AB, && (12)\\
(\phi\phi_g a)_t + \nabla\cdot(-D_a\phi\phi_g\nabla a) &= P(H\phi\phi_w A - \phi\phi_g a), && (13)\\
(\phi\phi_w B)_t + \nabla\cdot(-D_B\phi\phi_w\nabla B + \mathbf{q}B) &= f_{\mathrm{Diss}}\phi\phi_w - r\phi\phi_w m_B AB, && (14)\\
(\phi_s b)_t &= -f_{\mathrm{Diss}}\phi_s, && (15)\\
(\phi\phi_w C)_t + \nabla\cdot(-D_C\phi\phi_w\nabla C + \mathbf{q}C) &= -f_{\mathrm{Prec}}\phi\phi_w + r\phi\phi_w m_C AB, && (16)\\
(\phi_s c)_t &= f_{\mathrm{Prec}}\phi_s, && (17)\\
\phi_t &= s(\phi-\delta)\frac{1-\phi}{Z_\phi + (1-\phi)}(\phi_w f_{\mathrm{Diss}} - \phi_w f_{\mathrm{Prec}}), && (18)
\end{aligned}
$$

where $f_{\mathrm{Diss}} = S_{\mathrm{Diss}}(B_{eq} - B)$ and $f_{\mathrm{Prec}} = S_{\mathrm{Prec}}(C - C_{eq})$. These equations are defined in every $(t, \mathbf{x}) \in J \times Y$. The parameter s is just a switcher, for $s = 0$ the model is with constant porosity, whereas for $s \neq 0$ we have a variable porosity. The porosity decreases through precipitation and increases due to dissolution. Clearly, if (9) holds, then the mass-balance for a, i.e. (13) decouples from the rest of the system and can be therefore ignored in what follows. We remark that also the equations (15) and (17) are decoupled from the rest of the system and will be not considered in the next. Consequently, we will solve the equations for the water flow (10)-(11), for A, B and C (12), (14) and (16) and for the porosity (18). The numerical scheme based on MFEM is presented in Section 3. The initial conditions are given by $p|_{t=0} = p_I, A|_{t=0} = A_I, B|_{t=0} = B_I, C|_{t=0} = C_I, \phi|_{t=0} = \phi_I$ in Y. Boundary conditions complete the model.

Remark 2.1 *The rates on the right in the above model are only valid for physically reasonable regimes, i.e. whenever A, B and C are non-negative.*

Remark 2.2 *Notice that if δ is a (small) strictly positive constant, then the clogging of the pores cannot happen and the PDE system has a strongly non-linear, strongly coupled, and uniformly parabolic structure. On the other hand, if $\delta = 0$, then for some x and t the porosity $\phi(x,t)$ is zero. In such cases, the PDE system becomes strongly degenerate; note that the reaction-infiltration problem discussed in [9] exhibits a few conceptual similarities with our problem which we will exploit elsewhere. The term $\frac{1-\phi}{Z_\phi + (1-\phi)}$ ensures us that the porosity remains bounded from above by 1, with Z_ϕ being just a small positive constant.*

3 Numerical scheme based on MFEM

In order to state a MFEM scheme for the equations (10)-(11), (12), (14), (16) and (18) we have to introduce first the total mass fluxes of A, B and C:

$$
\begin{aligned}
\mathbf{q}_A &= -D_A\phi\phi_w\nabla A + \mathbf{q}A && (19)\\
\mathbf{q}_B &= -D_B\phi\phi_w\nabla B + \mathbf{q}B && (20)\\
\mathbf{q}_C &= -D_C\phi\phi_w\nabla C + \mathbf{q}C. && (21)
\end{aligned}
$$

In what follows we make use of common notations in the functional analysis. By $\langle\cdot,\cdot\rangle$ we mean the inner product on $L^2(Y)$, or the duality pairing between $H_0^1(Y)$ and $H^{-1}(Y)$. Further, $\|\cdot\|$ and $\|\cdot\|_1$ stand for the norms in $L^2(Y)$ and $H^1(Y)$, respectively. The functions in $H(\mathrm{div}; Y)$ are vector

valued, having a L^2 divergence. By c we mean a positive constant, not depending on the unknowns or the discretization parameters. We further use also the notation $\phi_{w,I} = \phi_w(p_I)$. Throughout this paper we make use of the following assumptions:

(A1) The conductivity function $k : [0,1] \to \mathbb{R}$ is strictly increasing, positive and Lipschitz continuous.

(A2) The initial concentrations A_I, B_I, and C_I are bounded and non-negative. The initial pressure p_I is bounded.

(A3) For both continuous and discrete cases there holds $1 \geq \phi\phi_w \geq \beta > 0$, and ϕ_w is Lipschitz continuous.

(A4) $\mathbf{q}, \mathbf{q}_A, \mathbf{q}_B, \mathbf{q}_C \in L^\infty(J \times Y) \cap L^2(J; H^1(Y))$ and $\partial_t p, \partial_t A, \partial_t B, \partial_t C \in L^\infty(J \times Y)$.

(A5) The reaction rates are Lipschitz continuous.

For simplicity, in this section we consider only homogeneous Dirichlet boundary conditions, but the results can be extended to more general cases. Throughout this paper we assume that the system (10)-(11), (12), (14), (16) and (18) complemented with boundary and initial conditions has a unique weak solution. This solves the following problem:

Problem 3.1 *(The continuous variational problem) Find* $p, A, B, C \in H^1(J; L^2(Y))$ *and* $\mathbf{q}, \mathbf{q}_A, \mathbf{q}_B, \mathbf{q}_C \in L^2(J; H(\mathrm{div}; Y))$ *with* $p|_{t=0} = p_I$, $A|_{t=0} = A_I$, $B|_{t=0} = B_I$, $C|_{t=0} = C_I$, $\phi|_{t=0} = \phi_I$ *such that*

$$
\begin{aligned}
\langle(\phi\phi_w)_t, w\rangle + \langle\nabla\cdot\mathbf{q}, w\rangle &= \langle\frac{\phi\phi_w}{\rho} rAB, w\rangle, && (22)\\
\langle K^{-1}(\phi\phi_w)\mathbf{q}, \mathbf{v}\rangle - \langle p, \nabla\cdot\mathbf{v}\rangle + \langle\nabla z, \mathbf{v}\rangle &= 0, && (23)\\
\langle(\phi\phi_w A)_t, w\rangle + \langle\nabla\cdot\mathbf{q}_A, w\rangle &= -\langle r\phi\phi_w m_A AB, w\rangle, && (24)\\
\langle(D_A\phi\phi_w)^{-1}\mathbf{q}_A, \mathbf{v}\rangle - \langle A, \nabla\cdot\mathbf{v}\rangle - \langle A\mathbf{q}, \mathbf{v}\rangle &= 0, && (25)\\
\langle(\phi\phi_w B)_t, w\rangle + \langle\nabla\cdot\mathbf{q}_B, w\rangle &= \langle f_{\mathrm{Diss}}\phi\phi_w, w\rangle - \langle r\phi\phi_w m_B AB, w\rangle, && (26)\\
\langle(D_B\phi\phi_w)^{-1}\mathbf{q}_B, \mathbf{v}\rangle - \langle B, \nabla\cdot\mathbf{v}\rangle - \langle B\mathbf{q}, \mathbf{v}\rangle &= 0, && (27)\\
\langle(\phi\phi_w C)_t, w\rangle + \langle\nabla\cdot\mathbf{q}_C, w\rangle &= -\langle f_{\mathrm{Prec}}\phi\phi_w, w\rangle + \langle r\phi\phi_w m_C AB, w\rangle, && (28)\\
\langle(D_C\phi\phi_w)^{-1}\mathbf{q}_C, \mathbf{v}\rangle - \langle C, \nabla\cdot\mathbf{v}\rangle - \langle C\mathbf{q}, \mathbf{v}\rangle &= 0, && (29)\\
\langle\phi_t, w\rangle &= s\langle\frac{(\phi-\delta)(1-\phi)}{Z_\phi + (1-\phi)}(\phi_w f_{\mathrm{Diss}} - \phi_w f_{\mathrm{Prec}}), w\rangle && (30)
\end{aligned}
$$

for all $w \in L^2(Y)$ *and* $\mathbf{v} \in H(\mathrm{div}; Y)$.

Referring strictly to the the Richards equation (22)–(23), existence and uniqueness results are obtained e.g. in [1]. For the system (24)–(29), existence and uniqueness can be proven by following [28] at least for the case when the diffusive flux does not contain $\phi\phi_w$ and the porosity is constant. These results are not straightforwardly applicable to the entire system (22) - (30), which might degenerate, therefore a further study is necessary.

For the time discretization we let $N \in \mathbb{N}$ be strictly positive, and define the time step $\tau = T/N$, as well as $t_n = n\tau$ ($n \in \{1, 2, \ldots, N\}$).Given a function f defined on the interval J, we write $f^n := f(t_n)$. Furthermore, we let $\mathcal{T}_h$ be a regular decomposition of $Y \subset \mathbb{R}^d$ into closed d-simplices; h stands for the mesh-size. Here we assume $\overline{Y} = \cup_{T\in\mathcal{T}_h} T$, hence Y is polygonal. We will use the discrete subspaces $W_h \subset L^2(Y)$ and $V_h \subset H(\mathrm{div}; Y)$ defined as

$$
\begin{aligned}
W_h &:= \{p \in L^2(Y) |\ p \text{ is constant on each element } T \in \mathcal{T}_h\},\\
V_h &:= \{\mathbf{q} \in H(\mathrm{div}; Y) |\ \mathbf{q}_{|T} = \mathbf{a} + b\mathbf{x} \ \text{ for all } T \in \mathcal{T}_h\}.
\end{aligned}
\tag{31}
$$

In other words, W_h denotes the space of piecewise constant functions, while V_h is the lowest order Raviart-Thomas RT_0 space (see [7]). We will use the following L^2 projector (see [7]):

$$P_h : L^2(Y) \to W_h, \qquad \langle P_h w - w, w_h \rangle = 0 \text{ for all } w \in L^2(Y),\ w_h \in W_h. \tag{32}$$

Applying a first order time stepping and MFEM, the fully discrete form of (22) - (30) reads

Problem 3.2 *(The discrete variational problem) Let $n \in \{1, \dots, N\}$, and $p_h^{n-1}, A_h^{n-1}, B_h^{n-1}, C_h^{n-1}, \phi_h^{n-1}$ be given. Find $p_h^n, A_h^n, B_h^n, C_h^n, \phi_h^n \in W_h$ and $\mathbf{q}_h^n, \mathbf{q}_{A_h}^n, \mathbf{q}_{B_h}^n, \mathbf{q}_{C_h}^n \in V_h$ such that for all $w_h \in W_h$ and $\mathbf{v}_h \in V_h$ there holds*

$$\langle \phi_h^n {\phi_w}_h^n - \phi_h^{n-1} {\phi_w}_h^{n-1}, w_h \rangle + \tau \langle \nabla \cdot \mathbf{q}_h^n, w_h \rangle = \tau \langle \frac{r}{\rho} \phi_h^{n-1} {\phi_w}_h^{n-1} A_h^{n-1} B_h^{n-1}, w_h \rangle, \tag{33}$$

$$\langle K^{-1}(\phi_h^n {\phi_w}_h^n) \mathbf{q}_h^n, \mathbf{v}_h \rangle - \langle p_h^n, \nabla \cdot \mathbf{v}_h \rangle + \langle \nabla z, \mathbf{v}_h \rangle = 0, \tag{34}$$

$$\langle \phi_h^n {\phi_w}_h^n A_h^n - \phi_h^{n-1} {\phi_w}_h^{n-1} A_h^{n-1}, w_h \rangle + \tau \langle \nabla \cdot \mathbf{q}_{A_h}^n, w_h \rangle = \tau \langle -m_A r \phi_h^n {\phi_w}_h^n A_h^n B_h^n, w_h \rangle, \tag{35}$$

$$\langle \frac{1}{D_A \phi_h^n {\phi_w}_h^n} \mathbf{q}_{A_h}^n, \mathbf{v}_h \rangle - \langle A_h^n, \nabla \cdot \mathbf{v}_h \rangle - \langle A_h^n \mathbf{q}_h^n, \mathbf{v}_h \rangle = 0, \tag{36}$$

$$\begin{aligned} \langle \phi_h^n {\phi_w}_h^n B_h^n - \phi_h^{n-1} {\phi_w}_h^{n-1} B_h^{n-1}, w_h \rangle + \tau \langle \nabla \cdot \mathbf{q}_{B_h}^n, w_h \rangle &= -\tau \langle m_B r \phi_h^n {\phi_w}_h^n A_h^n B_h^n, w_h \rangle \\ &\quad + \tau \langle \phi_h^n {\phi_w}_h^n {f_{\mathrm{Diss}}}_h^n, w_h \rangle, \end{aligned} \tag{37}$$

$$\langle \frac{1}{D_B \phi_h^n {\phi_w}_h^n} \mathbf{q}_{B_h}^n, \mathbf{v}_h \rangle - \langle B_h^n, \nabla \cdot \mathbf{v}_h \rangle - \langle B_h^n \mathbf{q}_h^n, \mathbf{v}_h \rangle = 0, \tag{38}$$

$$\begin{aligned} \langle \phi_h^n {\phi_w}_h^n C_h^n - \phi_h^{n-1} {\phi_w}_h^{n-1} C_h^{n-1}, w_h \rangle + \tau \langle \nabla \cdot \mathbf{q}_{C_h}^n, w_h \rangle &= \tau \langle m_C r \phi_h^n {\phi_w}_h^n A_h^n B_h^n, w_h \rangle \\ &\quad - \tau \langle \phi_h^n {\phi_w}_h^n {f_{\mathrm{Prec}}}_h^n, w_h \rangle, \end{aligned} \tag{39}$$

$$\langle \frac{1}{D_C \phi_h^n {\phi_w}_h^n} \mathbf{q}_{C_h}^n, \mathbf{v}_h \rangle - \langle C_h^n, \nabla \cdot \mathbf{v}_h \rangle - \langle C_h^n \mathbf{q}_h^n, \mathbf{v}_h \rangle = 0, \tag{40}$$

and

$$\langle \phi_h^n - \phi_h^{n-1}, w_h \rangle = \tau s \langle \frac{(\phi_h^{n-1} - \delta)(1 - \phi_h^{n-1})}{Z_\phi + (1 - \phi_h^{n-1})} ({\phi_w}_h^{n-1} {f_{\mathrm{Diss}}}_h^n - {\phi_w}_h^{n-1} {f_{\mathrm{Prec}}}_h^n), w_h \rangle, \tag{41}$$

where ${\phi_w}_h^k := \phi_w(p_h^k)$, ${f_{\mathrm{Diss}}}_h^k = S_{\mathrm{Diss}}(B_{eq} - B_h^k)$ and ${f_{\mathrm{Prec}}}_h^k = S_{Prec}(C_h^k - C_{eq})$, $k = 0, \dots, N$.

Initially we take $\phi_h^0 = P_h \phi_I$, p_h^0 so that holds $\phi_h^0 {\phi_w}_h^0 = P_h(\phi_I \phi_{w,I})$ and $A_h^0 = \dfrac{P_h(\phi_I \phi_{w,I} A_I)}{\phi_h^0 {\phi_w}_h^0}$, $B_h^0 = \dfrac{P_h(\phi_I \phi_{w,I} B_I)}{\phi_h^0 {\phi_w}_h^0}$ and $C_h^0 = \dfrac{P_h(\phi_I \phi_{w,I} C_I)}{\phi_h^0 {\phi_w}_h^0}$. The particular form of the initial data is allowed by the lower bound on $\phi \phi_w$ and will be used when proving Theorem 3.1 below.

Note that the equation (41) and the reaction in (33) are explicit. This suggests the following solution strategy, which has been adopted for the numerical calculations presented below. First of all, at each time we get the porosity from (41) and then solve (33)–(34), which is now decoupled from the remaining part of the system. Once a solution pair $(p_h^n, \mathbf{q}_h^n)$ is computed, one can proceed by determining $(A_h^n, \mathbf{q}_{A_h}^n)$, $(B_h^n, \mathbf{q}_{B_h}^n)$ and $(C_h^n, \mathbf{q}_{C_h}^n)$ by solving (35)–(40).

The convergence of the scheme presented in Problem 3.2 can be shown for constant porosity (i.e. $s = 0$) and strictly unsaturated flow, i.e. $\phi_w' > 0$ or fully saturated flow, e.g. $\phi_w = \phi_{w,\max}$ everywhere. In the next we will give convergence results for these two cases. We also briefly outline the proof for the former (which is by far much more interesting as the fully saturated case). The proof is based on techniques from [2] and [28].

Theorem 3.1 *(Strictly unsaturated flow) Let $s = 0$ and $p, A, B, C \in H^1(J; L^2(Y))$ and $\mathbf{q}, \mathbf{q}_A, \mathbf{q}_B$, $\mathbf{q}_C \in L^2(J; H(\mathrm{div}; Y))$ and $p_h^n, A_h^n, B_h^n, C_h^n \in W_h$, $\mathbf{q}_h^n, \mathbf{q}_{A_h}^n, \mathbf{q}_{B_h}^n, \mathbf{q}_{C_h}^n \in V_h$ solve Problem 3.1 and Problem 3.2, respectively. Assuming (A1) – (A5), there holds*

$$\begin{aligned}
&\|p(T) - p_h^n\|^2 + \sum_{n=1}^{N} \tau \|\mathbf{q}^n - \mathbf{q}_h^n\|^2 + \sum_{n=1}^{N} \tau \|A^n - A_h^n\|^2 \\
&+ \sum_{n=1}^{N} \tau \|B^n - B_h^n\|^2 + \sum_{n=1}^{N} \tau \|C^n - C_h^n\|^2 + \sum_{n=1}^{N} \tau \|\mathbf{q}_A{}^n - \mathbf{q}_{A_h}^n\|^2 \\
&+ \sum_{n=1}^{N} \tau \|\mathbf{q}_B{}^n - \mathbf{q}_{B_h}^n\|^2 + \sum_{n=1}^{N} \tau \|\mathbf{q}_C{}^n - \mathbf{q}_{C_h}^n\|^2 \leq c(\tau^2 + h^2).
\end{aligned} \tag{42}$$

Proof. Using the results from [29], which are obtained by the techniques from [2] one can show that for strictly unsaturated flow we have

$$\begin{aligned}
\|p(T) - p_h^n\|^2 + \sum_{n=1}^{N} \tau \|\mathbf{q}^n - \mathbf{q}_h^n\|^2 &\leq c(\tau^2 + h^2) \\
&+ c\Big(\sum_{n=1}^{N} \tau \|A^n - A_h^n\|^2 + \sum_{n=1}^{N} \tau \|B^n - B_h^n\|^2 + \sum_{n=1}^{N} \tau \|p^n - p_h^n\|^2\Big).
\end{aligned} \tag{43}$$

The next step is to prove a similar result for the remaining variables by applying the ideas in [28]. The main difficulty is but the appearance of ϕ_w in the terms which should furnish the L^2-norms of the flux variables in equations (25), (27), (29) and their discrete counterparts (36), (38), (40). To cope with this we use the elementary lemma

Lemma 3.1 *For any vectors $\mathbf{a}_k \in \mathbb{R}^d$ and scalars $b_k \in \mathbb{R}$, $(k \in \{1, \ldots, N\}, d \geq 1)$ we have*

$$2\sum_{n=1}^{N} \langle b_n \mathbf{a}_n, \sum_{k=1}^{n} \mathbf{a}_k \rangle = \langle b_N \sum_{n=1}^{N} \mathbf{a}_n, \sum_{n=1}^{N} \mathbf{a}_n \rangle + \sum_{n=2}^{N} \langle (b_{n-1} - b_n) \sum_{k=1}^{n-1} \mathbf{a}_k, \sum_{k=1}^{n-1} \mathbf{a}_k \rangle + \sum_{n=1}^{N} \langle b_n \mathbf{a}_n, \mathbf{a}_n \rangle. \tag{44}$$

The above lemma is an extension of the well known result for the case $b_k = 1$, for all $k \in \{1, \ldots, N\}$. By following [28], using the lemma above and the assumed regularity for the solution one has

$$\begin{aligned}
&\sum_{n=1}^{N} \tau \|A^n - A_h^n\|^2 + \sum_{n=1}^{N} \tau \|B^n - B_h^n\|^2 + \sum_{n=1}^{N} \tau \|C^n - C_h^n\|^2 \\
&+ \sum_{n=1}^{N} \tau \|\mathbf{q}_A{}^n - \mathbf{q}_{A_h}^n\|^2 + \sum_{n=1}^{N} \tau \|\mathbf{q}_B{}^n - \mathbf{q}_{B_h}^n\|^2 + \sum_{n=1}^{N} \tau \|\mathbf{q}_C{}^n - \mathbf{q}_{C_h}^n\|^2 \\
&\quad \leq c(\tau^2 + h^2 + \sum_{n=1}^{N} \tau \|\mathbf{q}^n - \mathbf{q}_h^n\|^2) \\
&\quad + c\Big(\sum_{n=1}^{N} \tau \|\phi_w(p^n) - \phi_w{}_h^n\|^2 + \sum_{n=1}^{N} \int_{t_{n-1}}^{t_n} \|\phi_w(p) - \phi_w{}_h^n\|^2\Big) \\
&\quad + c\Big(\sum_{n=1}^{N} \tau^2 \|\mathbf{q}_A{}^n - \mathbf{q}_{A_h}^n\|^2 + \sum_{n=1}^{N} \tau^2 \|\mathbf{q}_B{}^n - \mathbf{q}_{B_h}^n\|^2 + \sum_{n=1}^{N} \tau^2 \|\mathbf{q}_C{}^n - \mathbf{q}_{C_h}^n\|^2\Big).
\end{aligned} \tag{45}$$

By (43)–(45) and the discrete Gronwall Lemma we then get the result (42).

Q. E. D.

Theorem 3.2 *(Fully saturated flow) In the strictly saturated flow regime, the result (42) becomes*

$$\begin{aligned}\max_{n=1,\dots,N}\|p^n-p_h^n\|^2+\sum_{n=1}^{N}\tau\|\mathbf{q}(t_n)-\mathbf{q}_h^n\|^2+\max_{n=1,\dots,N}\|A^n-A_h^n\|^2\\ +\max_{n=1,\dots,N}\|B^n-B_h^n\|^2+\max_{n=1,\dots,N}\|C^n-C_h^n\|^2+\sum_{n=1}^{N}\tau\|{\mathbf{q}_A}^n-{\mathbf{q}_A}_h^n\|^2\\ +\sum_{n=1}^{N}\tau\|{\mathbf{q}_B}^n-{\mathbf{q}_B}_h^n\|^2+\sum_{n=1}^{N}\tau\|{\mathbf{q}_C}^n-{\mathbf{q}_C}_h^n\|^2\le c(\tau^2+h^2).\end{aligned}\tag{46}$$

4 Numerical illustration for the carbonation problem

We solve the equations (33)–(41) on $Y:=[0,1]\times[0,1]$. The initial pressure is given by $p=0.001(y-2)$. The boundary condition for the water flow are: Left, Right: zero flux and Up: $p=-0.001$, Down: $p=-0.002$ (so a flux is pointing downwards). For A,B and C we consider homogeneous Neumann boundary conditions. For simplicity, we do not take any gravitation effects into account. As mentioned in Section 2.2, we choose the parameterization of van Genuchten-Mualem as given in (6) – (7). The model parameters are chosen such as: $\rho=1$, $K_S=2.0$, $\phi_{w,\max}=0.5$, $\alpha=0.152$, $n=4.0$ $S_{\text{Diss}}=0.0067$, $B_{eq}=0.0075$, $S_{\text{Prec}}=0$, $C_{eq}=0$, $D_A=1.0$, $D_B=0.0864$ and $D_C=0.000864$. Further, we have $m_A=44, m_B=74, m_C=100.87$ and the regularization parameters $\delta=0.001, Z_\phi=0.01$. As initial conditions we take $A(\mathbf{x},0)=3*10^{-3}$ on Y_A^I, $A(\mathbf{x},0)=0$ on $Y\setminus Y_A^I$, $B(\mathbf{x},0)=0.0075$ on Ω_B^I, $B(\mathbf{x},0)=0$ on $Y\setminus Y_B^I$, and $C(\mathbf{x},0)=rA(\mathbf{x},0)B(\mathbf{x},0)$. For the porosity we take $\phi_I=0.5$. The physical units in this section are grams, centimeters and years and are not written every time explicitly. These values are realistic for the cement chemistry. For the initial domains Ω_A^I and Ω_B^I we consider three scenarios

$$(V1)\quad\begin{cases}Y_A^I=\{(x,y)\in Y|y\ge 0.5\}\\ Y_B^I=\{(x,y)\in Y|y\le 0.53\}\end{cases}\tag{47}$$

$$(V2)\quad\begin{cases}Y_A^I=\{(x,y)\in Y|(y\ge 0.5+0.4*x)\vee(y\ge 0.9-0.4*x)\}\\ Y_B^I=Y\setminus Y_A^I\end{cases}\tag{48}$$

$$(V3)\quad\begin{cases}Y_A^I=\{(x,y)\in Y|(y\ge 0.5-0.4*x)\wedge(y\ge 0.1+0.4*x)\}\\ Y_B^I=Y\setminus Y_A^I\end{cases}\tag{49}$$

Furthermore, A,B, and C are assumed to satisfy homogeneous Neumann boundary conditions across all sides of the square Y. For the degradation rate r we take successively the values: $10, 100$ and 1000. We compute numerically the indicator

$$\eta(t)=\int_Y rA(\mathbf{x},t)B(\mathbf{x},t)\,d\,\mathbf{x}.\tag{50}$$

and the mass flux of the species $i, i=A,B$ or C over the lower boundary Γ_S (the outflow boundary, given here by $x=0$)

$$mass_i(t)=\int_{\Gamma_S}\mathbf{q}_i\cdot n\,d\,s.\tag{51}$$

The numerical scheme (33)–(41) is implemented in the software package *UG* [4]. The computations are done with a time step $\tau=0.01$, on a regular triangular mesh with a diameter $h=0.02$ (5600 elements). For details of the implementation of the MFEM scheme for multicomponent, reactive transport in saturated/unsaturated media we refer to [27].

Fig. 1 and Fig. 2 illustrate the typical behavior of the concentrations A,B and C for one of our scenarios $(V3)$. As expected from the model equations, we notice the consumption of concentration A and subsequent production of concentration C. We also notice that, when choosing $r\ge 10$, we are actually simulating a reaction-diffusion-flow process in its fast-reaction regime (a high-Thiele-modulus

regime). This can be observed comparing the almost "complementarity" of the colors in Fig. 1 and Fig. 2. More precisely, we observe a high production of species C in those regions where A is strongly depleted. These pictures indicate therefore a separation in space of free A-molecules from B-molecules that are combined in C products. For low flow regimes, relying on singular-limit analyses such as [31], we expect that as $r \to \infty$ the production of C will localize on free interfaces separating pockets with A molecules from B-filled regions and $\eta \to 0$. For all three scenarios $V1 - V3$ we observe an initial increase of η till a maximum (the higher the peak, the higher the reaction rate r) and then a decrease to zero, see Fig. 3 – 6. The steepest decrease we see for the highest rate, $r = 1000$, independent of scenario. The behavior of η is very similar for all scenarios, see Fig. 3 – 6, the determinating facto being the reaction rate r. For $r = 1000$ very small values of η are reached already after short times (from 0.5 for scenario V1 to 0.8 for scenario V3), which is a strong indication of a sharp separation of species A and B, see Fig. 5 (right).

As one can see in Fig. 7 the model is very sensitive with respect to the dissolution rate S_{Diss} (a higher one implies much more production of the species B and also a higher maximum in η). In the same picture we can see but there is almost no influence of the precipitation rate S_{Prec} and of a variable porosity $(s = 1)$ on η. One reason for this is that the concentrations of A and B are relative small and so also the production of C and therefore the precipitation effect is neglectable. The same was confirmed also for a 1000-times higher water flux in Fig. 8 (left), where again is no difference on η between the simulations with or without a variable porosity. We looked also at the mass fluxes of species $A - C$ over the outflow boundary, as explained in (51). The results are presented in Fig. 8 (right) and Fig. 9. There is no difference between the computations with a variable porosity and the ones without $(s = 0)$.

5 Discussion

We considered a mathematical model for a prototypical reaction-diffusion-flow scenario in variable saturated porous media. The special features of our scenario are: the reaction produces water and therefore the flow and transport are coupled in both directions and moreover, the reaction may alter the microstructure. This means we have a variable porosity in our model. For the spatial discretization we propose a mass conservative scheme based on MFEM. More precisely, we use the lowest order Raviart-Thomas elements. The scheme is semi-implicit in time. Error estimates are obtained for some particular cases. We apply our finite element methodology for the case of concrete carbonation – one of the most important physico-chemical processes affecting the durability of concrete. We performed a sensitivity analysis by using realistic parameters from cement chemistry. The model is sensitive with respect to the reaction rate r and dissolution rate S_{Diss}. When the reaction rate $r \to \infty$, the indicator η tends rapidly to zero, therefore a sharp separation of the species A and B is documented. At least for the set of parameters we used we see no (short time) influence of the precipitation rate S_{Prec} and of a variable porosity. A reason for this is that for the considered scenarios the concentration of the species C (which might precipitate) is very, very small. A further study should follow.

References

[1] H. W. ALT AND S. LUCKHAUS, *Quasilinear elliptic-parabolic differential equations*, Math. Z. 183 (1983), pp. 311-341.

[2] T. ARBOGAST, M. OBEYESEKERE AND M. F. WHEELER, *Numerical methods for the simulation of flow in root-soil systems*, SIAM J. Num. Anal. 30 (1993), pp. 1677-1702.

[3] J. W. BARRETT AND P. KNABNER, *Finite Element Approximation of the Transport of Reactive Solutes in Porous Media. Part 1: Error Estimates for Nonequilibrium Adsorption Processes*, SIAM J. Numer. Anal. 34 (1997), pp. 201-227

[4] P. BASTIAN, K. BIRKEN, K. JOHANSSEN, S. LANG, N. NEUSS, H. RENTZ-REICHERT AND C. WIENERS, *UG–a flexible toolbox for solving partial differential equations*, Comput. Visual. Sci. 1 (1997), pp. 27-40.

[5] M. BAUSE AND P. KNABNER, *Numerical simulation of contaminant biodegradation by higher order methods and adaptive time stepping*, Comput. Visualiz. Sci. 7 (2004), pp. 61-78.

[6] J. BEAR AND Y. BACHMAT, *Introduction to Modelling of Transport Phenomena in Porous Media*, Kluwer Academic, Dordrecht, 1991.

[7] F. BREZZI AND M. FORTIN, *Mixed and Hybrid Finite Element Methods*, Springer-Verlag, New York, 1991.

[8] G. AUCHMUTY, J. CHADAM, E. MERINO, P. ORTOLEVA AND E. RIPLEY, *The structure and stability of propagating redox fronts*, SIAM J. Appl. Math. 46 (1986), pp. 588-604.

[9] X. CHEN AND J. CHADAM, *A reaction infiltration problem. part 1 - existence, uniqueness, regularity and singular limit in one space dimension*, Nonlinear Anal. TMA 27 (1996), pp. 463-49.

[10] C.J. VAN DUIJN AND I.S. POP, *Crystal dissolution and precipitation in porous media: pore scale analysis*, J. Reine Angew. Math. 577 (2004), pp. 171211.

[11] P. KNABNER, *Mathematische Modelle für Transport und Sorption gelöster Stoffe in porösen Medien*, Habilitationsschrift, Universität Augsburg, Germany, 1990.

[12] P. KNABNER, C. J. VAN DUIJN AND S. HENGST, *An analysis of crystal dissolution fronts in flows through porous media - part 1: Compatible boundary conditions*, Adv. Water Resour. 18 (1995), pp. 171185.

[13] M. VAN GENUCHTEN, *A closed-form equation for predicting the hydraulic conductivity of unsaturated soils*, Soil Sci. Soc. Am. 44 (1980), pp. 892-898.

[14] J. KAČUR AND R. VAN KEER, *Solution of contaminant transport with adsorption in porous media by the method of characteristics*, M2AN 35 (2001) pp. 981-1006.

[15] R. KLÖFKORN, D. KRÖNER AND M. OHLBERGER, *Local adaptive methods for convection dominated problems*, Internat. J. Numer. Methods in Fluids 40 (2002), pp. 79-91.

[16] K. KUMAR, T. L. VAN NOORDEN AND I. S. POP, *Effective dispersion equations for reactive flows involving free boundaries at the micro-scale*, Multiscale Model. Simul. 9 (2011), pp. 29-58.

[17] W. K. LEWIS AND W. G. WHITMAN, *Principles of gas absorption*, Ind. Eng. Chem. Res. 16 (1924), 1215-1220.

[18] S. A. MEIER, M.A. PETER, A. MUNTEAN AND M. BÖHM, *Dynamics of the internal reaction layer arising during carbonation of concrete*, Chemical Engineering Science 62 (2007), pp. 1125-1137.

[19] R. MOSE, P. SIEGEL, P. ACKERER AND G. CHAVENT, *Application of the mixed hybrid finite element approximation in a groundwater flow model: Luxury or necessity ?*, Water Resources Research 30 (1994), pp. 3001-3012.

[20] Y. MUALEM, *A new model for predicting hydraulic conductivity of unsaturated porous media*, Water Resour. Res. 12 (1976), pp. 513-522.

[21] T. L. VAN NOORDEN, *Crystal precipitation and dissolution in a porous medium: effective equations and numerical experiments*, Multiscale Model. Simul. 7 (2008), pp. 12201236.

[22] T. L. VAN NOORDEN AND I. S. POP, *A Stefan problem modelling dissolution and precipitation*, IMA J. Appl. Math. 73 (2008), pp. 393411.

[23] T. L. VAN NOORDEN, I. S. POP, A. EBIGBO, AND R. HELMIG, *An upscaled model for biofilm growth in a thin strip*, Water Resour. Res. 46 (2010), W06505, doi:10.1029/2009WR008217.

[24] M. OHLBERGER AND C. ROHDE, *Adaptive finite volume approximations of weakly coupled convection dominated problems*, IMA J. Numer. Anal. 22 (2002), pp. 253-280.

[25] P. ORTOLEVA, *Geochemical Self-Organization*, Vol. 23 of Oxford Monographs on Geology and Geophysics, Oxford University Press, NY, Oxford, 1994.

[26] M.A. PETER, A. MUNTEAN, S.A. MEIER AND M. BÖHM, *Competition of several carbonation reactions in concrete: A parametric study*, Cement and Concrete Research 38 (2008), pp. 1385-1393.

[27] F. A. RADU, M. BAUSE, A. PRECHTEL AND S. ATTINGER, *A mixed hybrid finite element discretization scheme for reactive transport in porous media*, Numerical Mathematics and Advanced Applications, K. Kunisch, G. Of and O. Steinbach (editors), Springer Verlag, 2008, pp. 513-520.

[28] F. A. RADU, I. S. POP AND S. ATTINGER, *Analysis of an Euler implicit - mixed finite element scheme for reactive solute transport in porous media*, Numer. Meth. PDE's 26 (2009), pp. 320-344.

[29] F. A. RADU AND W. WANG, *Convergence analysis for a mixed finite element scheme for flow in strictly unsaturated porous media*. Nonlinear Analysis Serie B: Real World Applications (2011), DOI:10.1016/j.nonrwa.2011.05.003.

[30] B. RIVIERE AND M. F. WHEELER, *Discontinuous Galerkin methods for flow and transport problems in porous media*, Communications in numerical methods in engineering 18 (2002), pp. 63-68.

[31] T. SEIDMAN, *Interface conditions for a singular reaction-diffusion system*, DCDS B 2 (2009), pp. 631-643.

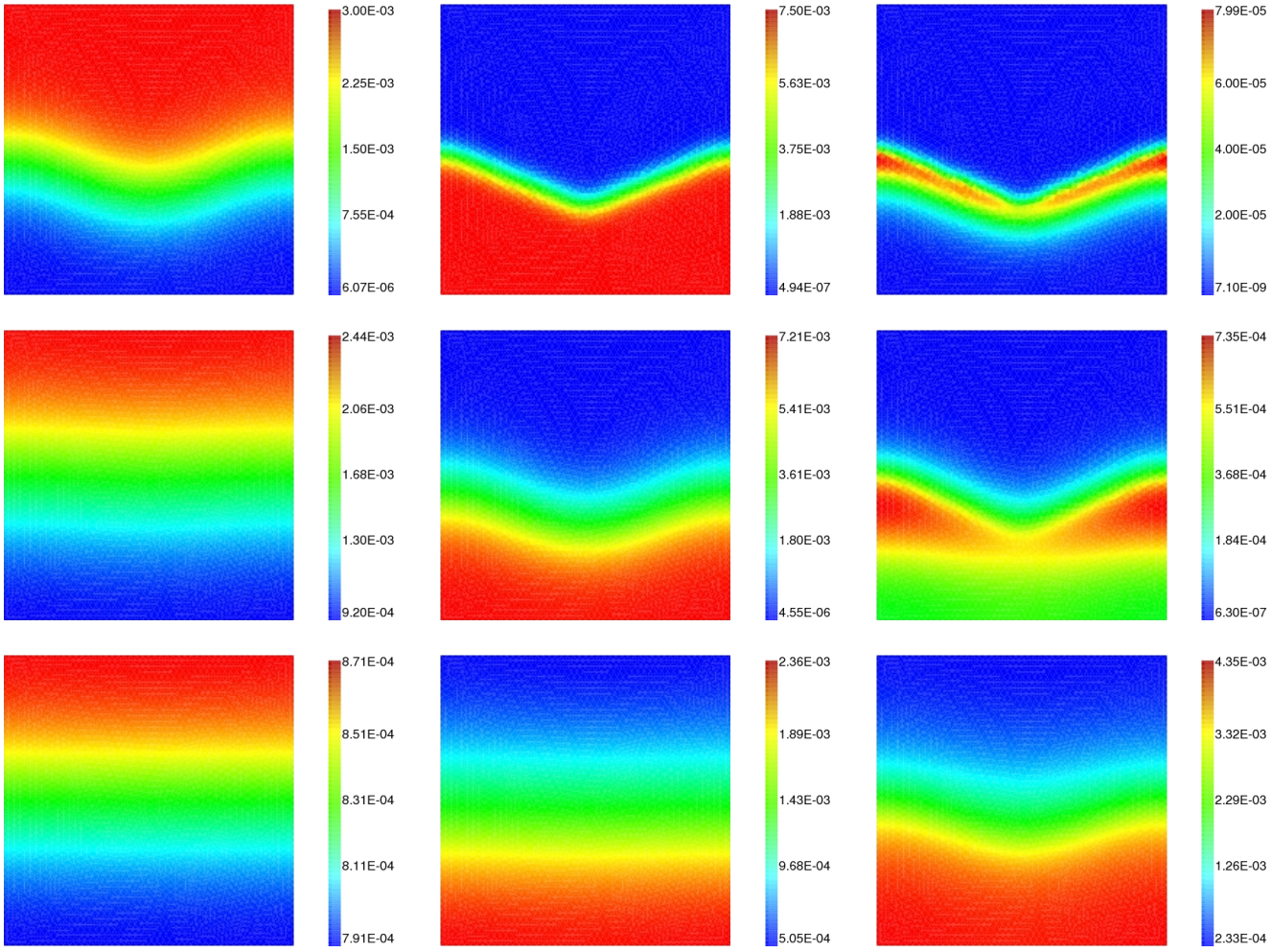

Figure 1: Concentration profiles of A, B and C at time $T = 0.01, T = 0.1$ and $T = 1$ for the scenario $V3$ with $r = 10$.

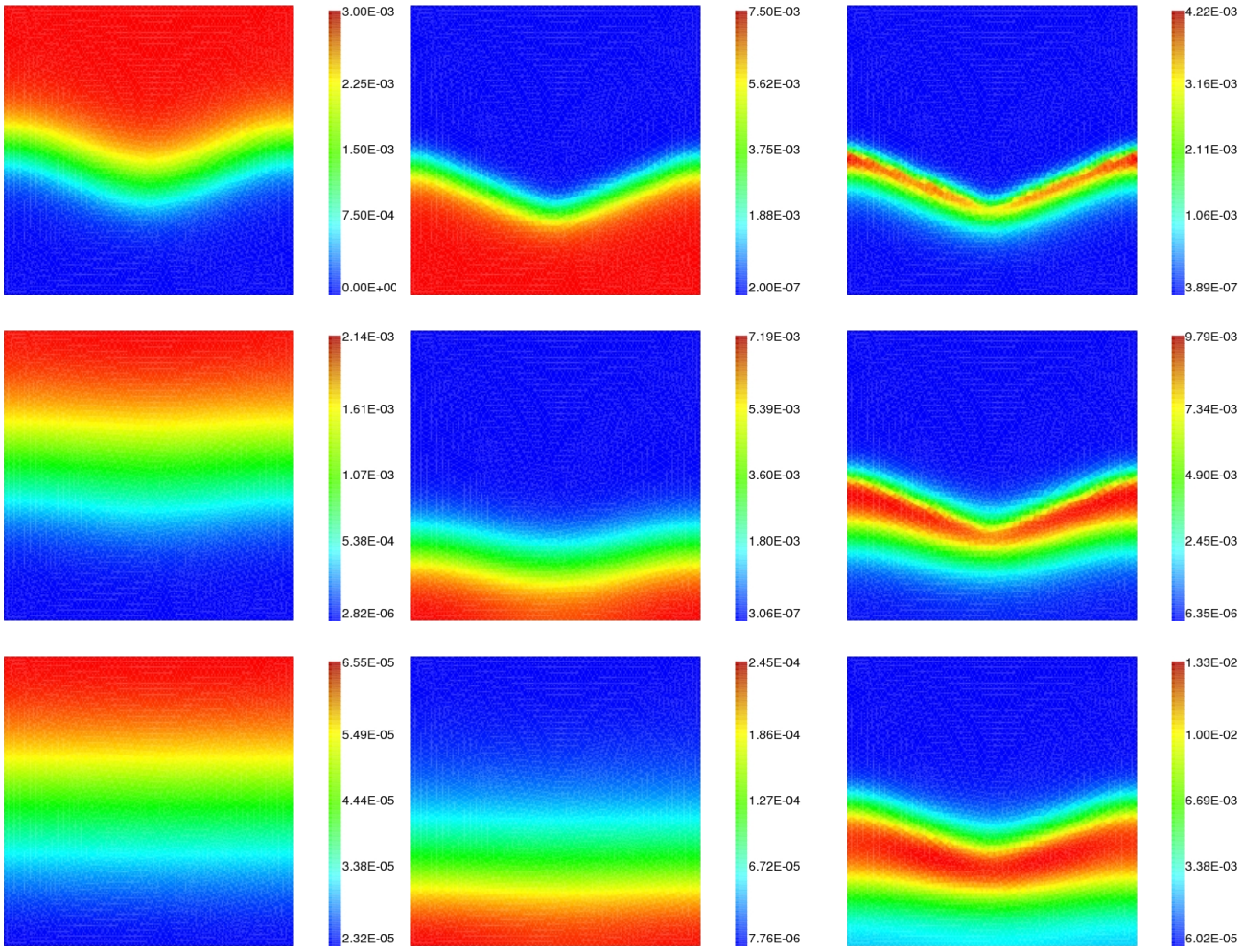

Figure 2: Concentration profiles of A, B and C at time $T = 0.01, T = 0.1$ and $T = 1$ for the scenario $V3$ with $r = 1000$.

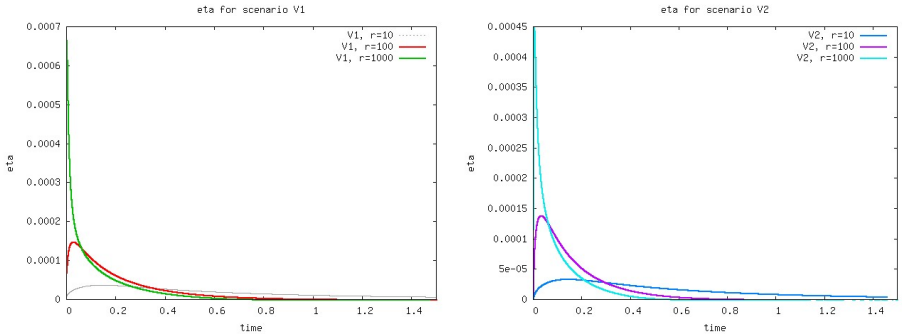

Figure 3: The indicator η for scenario $V1$ (left) and $V2$ (right)

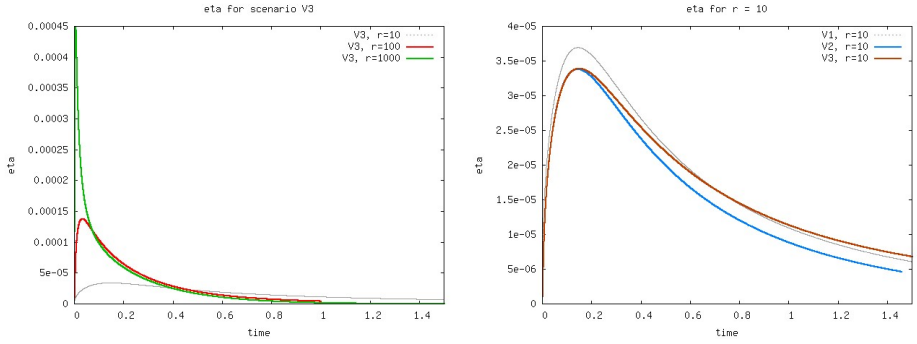

Figure 4: The indicator η for scenario $V3$ (left) and $r = 10$ (right)

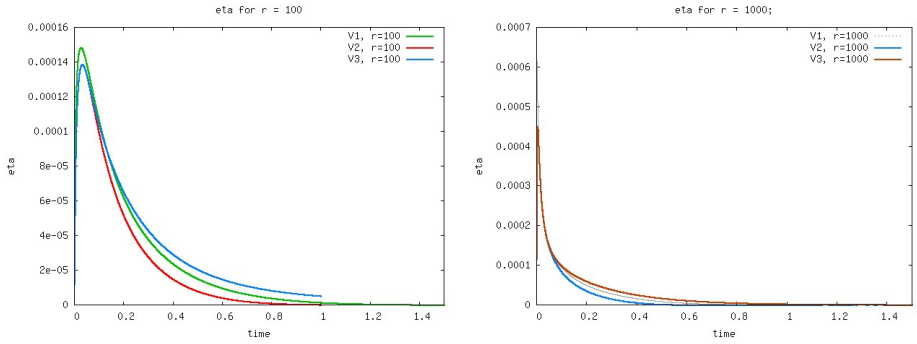

Figure 5: The indicator η for $r = 100$ (left) and for $r = 1000$ (right)

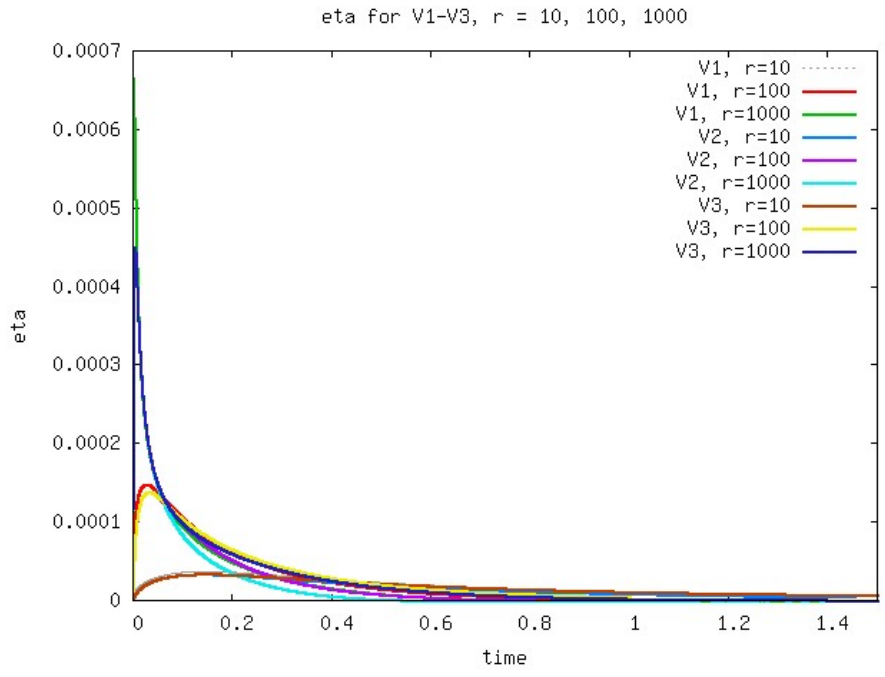

Figure 6: The indicator η for scenarios $V1 - V3$ and rates $r = 10, 100, 1000$

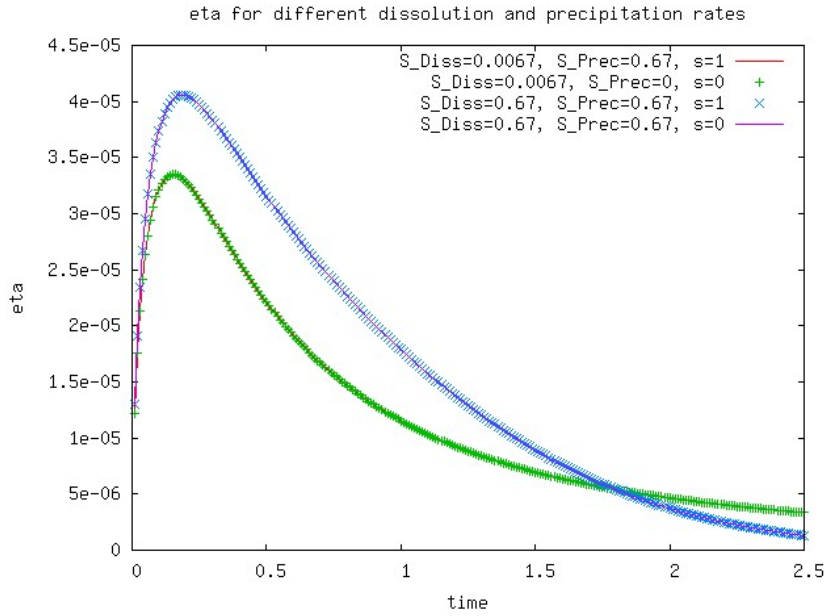

Figure 7: The indicator η for $V3$, rate $r = 10$, different dissolution and precipitation rates and with ($s = 1$) or without ($s = 0$) variable porosity

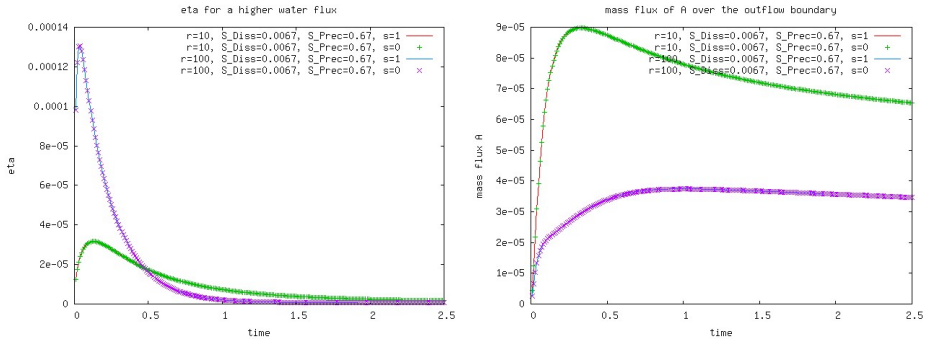

Figure 8: Simulations for scenario $V3$ with a 1000-times enhanced water flux for $r = 10$ and $r = 100$, with ($s = 1$) or without ($s = 0$) variable porosity: the indicator η (left) and the mass flux of A over the outflow boundary (right)

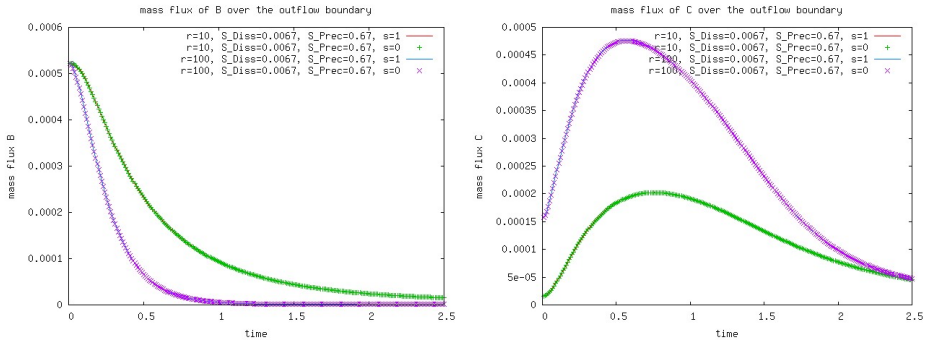

Figure 9: Simulations for scenario $V3$ with a 1000-times enhanced water flux for $r = 10$ and $r = 100$, with ($s = 1$) or without ($s = 0$) variable porosity: the mass flux of B over the lower boundary (left) and the mass flux of C over the outflow boundary (right)

PREVIOUS PUBLICATIONS IN THIS SERIES:

Number	Author(s)	Title	Month
11-45	J. de Graaf	A complex-like calculus for spherical vectorfields	Sept. '11
11-46	C. Cancès I.S. Pop M. Vohralík	An a posterior error estimate for vertex-centered finite volume discretizations of immiscible incompressible two-phase flow	Sept. '11
11-47	M.H.A. van Geel C.G. Giannopapa B.J. van der Linden J.M.B. Kroot	Development of a blood flow model including hypergravity and validation against an analytical model	Sept. '11
11-48	M.H.A. van Geel C.G. Giannopapa B.J. van der Linden	Development of a blood flow model and validation against experiments and analytical models	Sept. '11
11-49	F.A. Radu A. Muntean I.S. Pop N. Suciu O. Kolditz	A mixed finite element discretization scheme for a concrete carbonation model with concentration-dependent porosity	Sept. '11

Ontwerp: de Tantes,
Tobias Baanders, CWI